Letter

Unified view of elastic and elasto-inertial turbulence in channel flows at low and moderate Reynolds numbers

Giulio Foggi Rota,[1] Christian Amor,[1] Soledad Le Clainche,[2] and Marco Edoardo Rosti[1,*]

[1]*Complex Fluids and Flows Unit, Okinawa Institute of Science and Technology Graduate University, 1919-1 Tancha, Onna-son, Okinawa 904-0495, Japan*

[2]*School of Aerospace Engineering, Universidad Politécnica de Madrid, E-28040 Madrid, Spain*

(Received 25 March 2024; accepted 6 December 2024; published 30 December 2024)

The chaotic flow of elastic fluids at low Reynolds number (*Re*) is typically distinguished into elasto-inertial and elastic turbulence (EIT/ET). However, the clear separation among these two turbulent regimes in parallel flows with a gradual *Re* decrease remains elusive. Here, spanning *Re* over four orders of magnitude, we investigate the statistical and structural nature of the flows computed by fully resolved 3D numerical simulations, revealing that as inertia becomes subdominant all flows share similar dynamical properties. Supported by the results, we thus propose a unified view of fully developed ET and EIT in parallel flows.

DOI: 10.1103/PhysRevFluids.9.L122602

Turbulence is an open problem in fluid transport applications, as it significantly enhances the drag and energy expenditures. Nevertheless, it is beneficial in mixing problems since it introduces an additional diffusion mechanism on top of the classical viscous one. Indeed, viscous diffusion is often too slow for practical applications, but it is the only mechanism operating in low Reynolds number flows, which are typically laminar. The Reynolds number, *Re*, is the non dimensional parameter conventionally adopted to describe fluid flow, representing the relative importance of inertia compared to viscosity. Microscale mixing in low Reynolds number flows is a widely investigated research topic [1–3] for its high biological relevance, e.g., in drug delivery applications [4] and in the analysis of specimens for disease diagnosis [5]. Among the various mixing techniques, one is to exploit elastic turbulence [6], a peculiar chaotic state unique of viscoelastic fluids which are characterized by the coexistence of viscous and elastic effects.

The description of viscoelastic fluid flows necessitates an additional parameter accounting for the ratio of the elastic and flow time scales: the Deborah number, *De*. Comparing the Deborah to the Reynolds number allows to identify distinct regimes of motion: when inertial effects are dominant, turbulent drag reduction [7] (TDR) occurs, while elastic turbulence [8] (ET) is observed for dominant elasticity. In between these two extrema, an intermediate state dubbed elasto-inertial turbulence [9] (EIT) has been usually identified, where both elastic and inertial effects are relevant. There is no universal consensus on the definitions of EIT and ET; yet, for the purposes of our investigation, we follow Groisman and Steinberg [8] and denote with ET the chaotic flow observed in polymer solutions at small values of *Re* and large values of *De* ($Re \lesssim De$). Furthermore, according

*Contact author: marco.rosti@oist.jp

Published by the American Physical Society under the terms of the Creative Commons Attribution 4.0 International license. Further distribution of this work must maintain attribution to the author(s) and the published article's title, journal citation, and DOI.

to the definition given by Samanta *et al.* [10] recently adopted also by Dubief *et al.* [9], we dub EIT the chaotic motion controlled by the elastic stresses that can set in at lower Reynolds number than inertial turbulence, in a parameter range where inertia cannot be neglected ($Re \approx De$). Similarly, Page *et al.* [11] defined EIT as a new turbulent flow state observed at modest inertia and elasticity, while Khalid *et al.* [12] dubbed EIT the ensuing flow state to which pipe and channel flows of sufficiently elastic polymer solutions transition from the laminar state at Reynolds numbers substantially lower than the typical Newtonian threshold.

EIT occurs at significantly lower Reynolds numbers than TDR, where the laminar flow of a Newtonian fluid would be linearly stable, and it is characterized by different dynamical properties [10]. When inertial effects vanish, the flow can still become turbulent (ET) due to the onset of different elastic instabilities. It is in fact well established that different instability mechanisms are responsible for the transition to a chaotic state at moderate [13] and vanishing [14] values of Re, thus motivating the distinction between EIT and ET in the stability framework [9]. In curvilinear wall bounded flows, ET is triggered and sustained by a force directed as the flow curvature, called hoop stress [8,15]. Recent experiments [16,17] and numerical simulations [18,19] have highlighted that ET can also be attained in parallel shear flows, but a comprehensive characterization of its mechanisms is still elusive. After the discovery of a linear elastic instability in the parallel Kolmogorov flow [20], the weakly nonlinear regime following the instability has been studied [21] and observed to culminate in ET [22]. Arrowhead-shaped traveling elastic waves were first observed in this scenario [14] and later found also in the bulk of channel flows in the EIT [13,23–25] and ET regimes [26], suggesting a possible continuous path between the two [9] and hinting toward the existence of a unique sustainment mechanism common to EIT and ET [12]. Channel flows at moderate to vanishing inertia have been recently observed to share also a different instability [27], localized close to the walls. Nevertheless, due to a lack of measurements, it is still unclear if the fully developed three-dimensional EIT and ET chaotic states are the same, connected or completely decoupled.

In this Letter we show that fully developed EIT and ET in planar channel flows below $Re \approx 2800$share a similar structure, notwithstanding the instabilities leading to them. Addressing the fundamental question "Is EIT simply an inertial version of ET or does inertia play a more fundamental role?" posed by Dubief *et al.* [9], we thus clarify the relation between EIT and ET within this setup. Our fully resolved three-dimensional numerical simulations, spanning Reynolds numbers over four orders of magnitude (as in Fig. 1), allow us to bridge the different regimes (TDR, EIT, and ET) and clarify their relation. For every Reynolds number considered in this study we observe the system to converge toward a self-sustained chaotic state even when the flow of a Newtonian fluid would instead be laminar, and we identify only two different regimes, one at large Reynolds number (TDR) and one at smaller ones (ET).

To show this, we simulate the flow of a viscoelastic incompressible fluid between two indefinite planar walls at a distance of $2h$ from each other, described in a Cartesian coordinate frame with the x, y, and z axes aligned with the streamwise, wall-normal, and spanwise directions, respectively. Variables and symbols are listed in Sec. V of the Supplemental Material. The system is governed by the conservation of mass and momentum,

$$\boldsymbol{\nabla} \cdot \mathbf{u} = 0, \tag{1}$$

$$\rho(\partial_t \mathbf{u} + \boldsymbol{\nabla} \cdot \mathbf{uu}) = -\boldsymbol{\nabla} p + \mu_s \boldsymbol{\nabla} \cdot (\boldsymbol{\nabla}\mathbf{u} + (\boldsymbol{\nabla}\mathbf{u})^T) + \rho\mathbf{f} + \boldsymbol{\nabla} \cdot \mathbf{T}, \tag{2}$$

where $\mathbf{u}$ is the velocity, ρ the density, p the pressure, and μ_s the dynamic viscosity of the Newtonian solvent in which the polymer molecules are dissolved. $\mathbf{f}$ represents the forcing term needed to drive the flow at a constant flow rate, while $\mathbf{T}$ is the tensor accounting for the non-Newtonian behavior. In our study, $\mathbf{T}$ derives from a finitely extensible nonlinear elastic model with Peterlin's closure (FENE-P [28], equivalent to a bead-spring-type model [29]) and relates to the polymer conformation tensor, $\mathbf{C}$, as $\mathbf{T}(\mathbf{C}) = (\mu_p/\lambda)(f(tr(\mathbf{C}))\mathbf{C} - (L^2_{\max}\mathbf{I})/(L^2_{\max} - 3))$, where $L_{\max}$ denotes the maximum extensibility of the polymer chains, $\mathbf{I}$ is the tensorial identity, μ_p is the dynamic viscosity of the

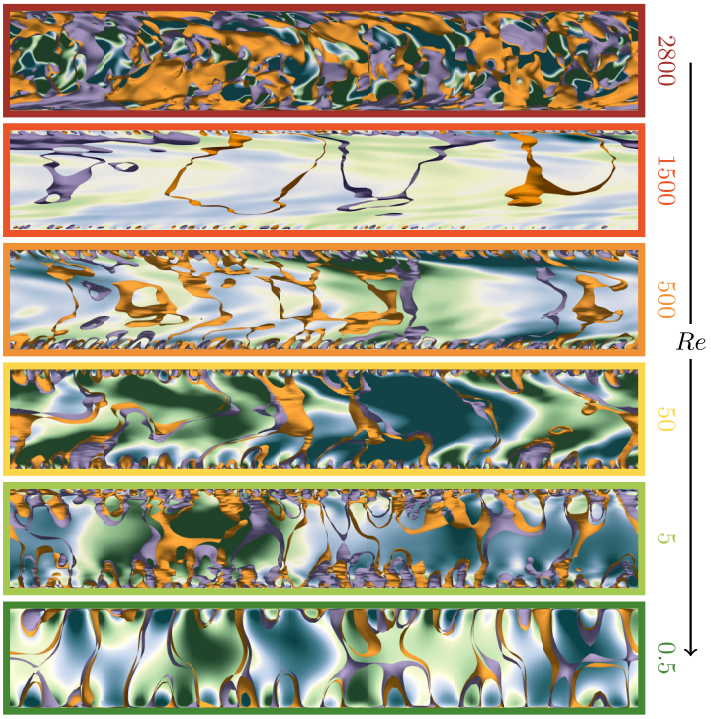


FIG. 1. Side views of the channel, with the mean flow going from left to right. We show the spanwise velocity fluctuations normalized with the mean turbulent kinetic energy, $w'/\sqrt{K}$, ranging from -0.3 (blue) to 0.3 (green); superimposed are the local isosurfaces of the wall-normal fluctuations, $v'/\sqrt{K}$, at -0.05 (orange) and $+0.05$ (violet).

polymer, and λ is its relaxation time. In particular, $f(s) = L_{\max}^2/(L_{\max}^2 - s)$. Finally, $\mathbf{C}$ evolves in time according to its own transport equation

$$\partial_t \mathbf{C} + (\mathbf{u}\cdot\nabla)\mathbf{C} - \mathbf{C}\cdot\nabla\mathbf{u} - (\nabla\mathbf{u})^T\cdot\mathbf{C} = -\tfrac{1}{\lambda}(f(tr(\mathbf{C}))\mathbf{C} - \mathbf{I}). \tag{3}$$

The regime of motion of the viscoelastic fluid is identified by the specification of the Reynolds and the Deborah numbers, along with the solvent-to-total viscosity ratio, β, and $L_{\max}$. In this work we adopt the definition of "bulk" Reynolds number, $Re = hU/\nu$, based on the mean velocity within the channel, U, and the total kinematic viscosity of the polymeric solution, $\nu = (\mu_s + \mu_p)/\rho$; we therefore decrease Re in $\{2800, 1500, 500, 50, 5, 0.5\}$ starting from the upper bound for EIT reported by Dubief *et al.* [9]. Furthermore, we complement our results with those available in the literature by Lellep *et al.* [19] at even smaller Reynolds number, $Re = 0.01$. The Deborah number is defined as $De = \lambda U/h$ and imposed equal to 50 throughout the whole study, while $L_{\max}$ and $\beta = \mu_s/(\mu_s + \mu_p)$ are set to 500 and 0.9, respectively. We start each simulation from a fully developed field of the closest case at a higher Reynolds number, and advance it in time according to the methods detailed in Sec. I of the Supplemental Material [30]. Our parameters are chosen consistently with previous stability analysis [25] and yield values of the elasticity number $El = De/Re$ in $\{0.02, 0.03, 0.1, 1, 10, 100\}$, denoting how the investigated range equally encompasses cases dominated by inertia ($El \ll 1$) and elasticity ($El \gg 1$), as well as the intermediate range. The results presented in the following have been replicated also with the Oldroyd-B liquid, thus proving their robustness against the polymer model adopted; furthermore, we have tested the effect of different viscosity ratios β, as detailed in Sec. IV of the Supplemental Material.

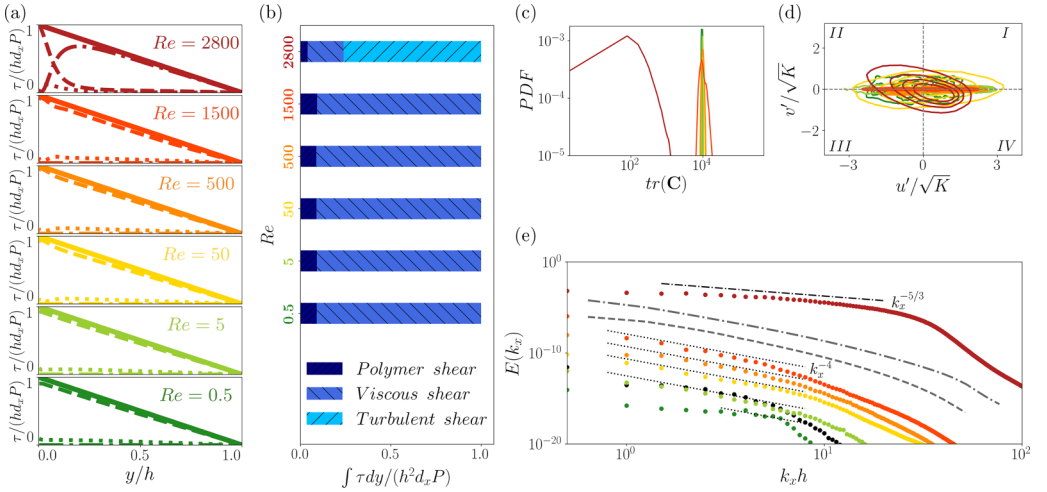


FIG. 2. Flow statistics. In (a) we report the viscous (dashed), turbulent (dashed-dotted) and polymer (dotted) shears, summing up to the total shear stress τ (solid line). At $Re \leqslant 1500$, viscosity and elasticity dominate throughout the whole half-channel height h. All the contributions integrated along the wall-normal direction, in (b), are thus dominated by the viscous and polymer shears, but for the case at $Re = 2800$, dominated by the turbulent shear. Consistently, the polymer stretching is enhanced, as shown in (c) by the PDFs of the trace of $\mathbf{C}$ at the channel centerline: their barycenters are far from $tr(\mathbf{C}) = 3$. (d) shows the J-PDFs of the normalized streamwise and wall-normal velocity fluctuations at $y = h/2$, at $\{0.1, 0.3, 0.5, 0.7\}$ of their maximum. The typical turbulent shape is recovered at $Re = 2800$, while in all the other cases the fluctuations decorrelate. We show the TKE spectra (e) with an arbitrary vertical shift, to prevent their overlapping, along with Oldroyd-B data at $Re = 5$ (black circles) and data from Lellep *et al.* [19] at $Re = 0.01$ and $De = 80/150$ as a gray dashed/dash-dotted line, respectively. The -4 slope contrasts sharply with the $-5/3$ decay observed in TDR, pointing toward a unified view of EIT and ET.

At all the Reynolds numbers but the highest one, qualitatively similar coherent fluctuations of the velocity are superimposed to a mean flow which only slightly departs from the laminar one (see more details on this in Sec. II of the Supplemental Material). As visible in Fig. 1, large structures span the center of the domain, while smaller ones characterize the region near the wall. All of them exhibit a quasiperiodic spatial arrangement superimposed to random perturbations. A more quantitative characterization of the flow fields is attained looking at the balance of the total shear stress, τ, along the half-channel height, h. The conservation of linear momentum requires the wall-normal derivative of τ to balance the driving pressure gradient, $d_y\tau = d_xP$, imposing a linear trend of τ with y. Three different contributions sum together in the total shear stress: a polymeric one due to the shearing component of the viscoelastic stresses $\mathbf{T}$ ($\langle T_{xy}\rangle$, where angle brackets denote averaging in time and along the homogeneous directions), a purely viscous one coming from the mean velocity profile $\langle u\rangle$ ($\rho\nu\partial_y\langle u\rangle$), and a turbulent one caused by the correlated fluctuations of the streamwise and wall-normal velocities ($-\rho\langle u'v'\rangle$, where the primes indicate fluctuations). These contributions are reported in the plots of Fig. 2(a).

As expected for the TDR regime at $Re = 2800$, the viscoelastic contribution remains small almost everywhere and viscosity is mostly relevant close to the wall, while the turbulent contribution dominates the center of the channel. For $Re \leqslant 1500$, instead, the shear stress balance is completely different, as the polymer and viscous shears become relevant throughout the channel and the turbulent one is depleted. To better weight the relative importance of the different contributions of the shear stress balance, we integrate the momentum balance along the wall-normal direction $[\int (\langle T_{xy}\rangle + \rho\nu\partial_y\langle u\rangle - \rho\langle u'v'\rangle)dy = h^2 \ d_xP]$, as represented graphically in Fig. 2(b). The turbulent shear is the most relevant component at $Re = 2800$, while it is practically zero in all the other

cases; those are dominated by the viscous shear, along with a non-negligible polymeric contribution (individually shown in Sec. II of the Supplemental Material). Significantly, the relative amplitude of the different contributions remains unchanged for all the Reynolds numbers (ET) but the highest one (TDR).

The previous results warrant two important clarifications. First, the relative small contribution of the polymers does not mean that the polymers are not stretched. Indeed, the polymer molecules are significantly stretched regardless of the case considered, as shown by the probability density functions (PDF) of the trace of $\mathbf{C}$ reported in Fig. 2(c). Also here, a clear separation can be appreciated between the case at $Re = 2800$ and all the others. Second, the vanishing magnitude of the turbulent shear when $Re \leqslant 1500$ does not mean that the turbulent fluctuations disappear, but rather suggests that the streamwise and wall-normal velocity fluctuations decorrelate. We therefore compute the joint probability density function (J-PDF) of the streamwise and wall-normal velocity fluctuations at a wall distance of $h/2$, reported in Fig. 2(d), where velocities are made dimensionless with the mean turbulent kinetic energy in the channel, K, for a better comparison of the different Reynolds numbers. In the high Reynolds case the isolines exhibit an oval shape with the major axis inclined downward, denoting a negative correlation among the two velocity components, and ejections ($u' < 0$, $v' > 0$) dominate over sweeps ($u' > 0$, $v' < 0$), analogously to the Newtonian case [43]. At this wall distance, the J-PDF peaks in the fourth quadrant. This picture completely changes when decreasing the Reynolds number, as the streamwise velocity decorrelates from the wall-normal one and its fluctuations heavily dominate in intensity; the J-PDF consequently appears flattened along the x axis, explaining the apparent disappearance of the turbulent shear stress from Fig. 2.

The features of the low Reynolds flow fields described up to this point would appear compatible with an incomplete relaminarization of the flow; nevertheless, its turbulent nature is confirmed by the full multiscale Fourier's spectra E of the turbulent kinetic energy (TKE) at the centerline of the channel. Those are characterized by a power-law decay of $E(k_x) \sim k_x^{-4}$ over roughly a decade of streamwise wave numbers k_x [Fig. 2(e), in good agreement with recent observations in a similar setup at lower Reynolds number [19] and in homogeneous isotropic elastic turbulence [44]. The wavenumber range in which the scaling is observed extends moving from $Re = 1500$ to $Re = 50$, yet it appears significantly shrank at $Re = 0.5$, suggesting a tendency of the flow to relaminarize at even lower Reynolds numbers. This is consistent with recent stability analysis results [25,42] considering our same polymer model (FENE-P) and same parameter range (Reynolds number, Deborah number, polymer concentration, and maximum extensibility). In the TDR regime at $Re = 2800$, instead, our data exhibit a tendency toward the conventional $E(k_x) \sim k_x^{-5/3}$ trend expected for Newtonian turbulence at high Reynolds number. Once more, no significant difference is observed among all the low Reynolds number cases; the robustness of this statement to significant variations of the polymer concentration is detailed in Sec. IV of the Supplemental Material. Our results therefore point toward a unified view of EIT and ET in three-dimensional fully developed planar channel flows below $Re \approx 2800$.

To further confirm this scenario, we apply a purely data-driven algorithm to identify and extract the coherent structures in the flow at different Reynolds numbers. In particular, we adopt the higher order dynamic mode decomposition [39], a dimensionality reduction algorithm which provides a finite set of modes, each oscillating in time with a specific frequency ω. Past stability analysis of viscoelastic two-dimensional channel flows suggests that traveling waves originated at a relatively high-Re bifurcation [13] persist in EIT [11,24,25,45] and ET [26,42]. These structures are mainly located away from the walls, in the central region of the channel, and are sometimes termed "arrowheads" [11]. In ET, these coexist with a recently discovered wall-localized linear instability caused by the presence of small but nonzero diffusivity of the polymer stresses [27,41]. The diffusive instability perturbs the flow close to the walls, in the region where the traveling waves convert most of the kinetic energy into elastic energy [36]. Our analysis suggests that all the turbulent flows at $Re \leqslant 1500$ can be described by the superposition of two main sets of modes for all the Reynolds numbers but the highest one, once more corroborating the unified view of EIT and ET suggested

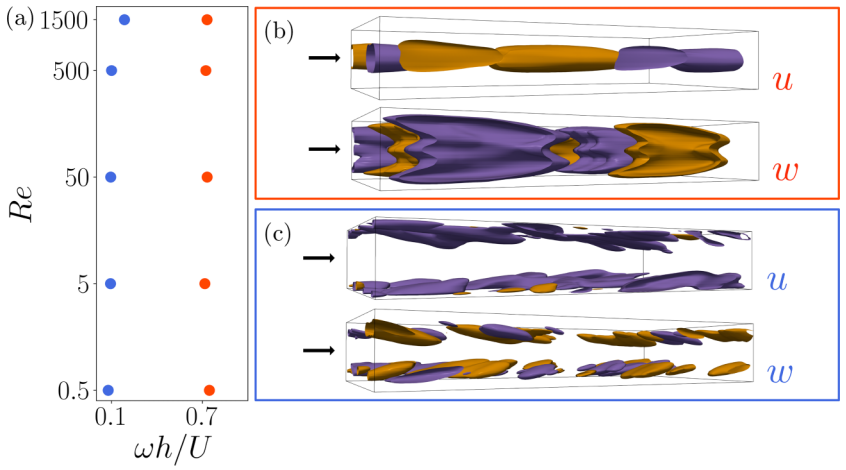


FIG. 3. Modal decomposition. showing the temporal frequencies (a), ω, of the two most dynamically relevant modes (b), (c) for five different values of the Reynolds number. The uncertainty of the decomposition algorithm calibration process lays within the symbols (see Sec. III of the Supplemental Material). The colored panels (b), (c) report the typical shapes of the streamwise, u, and spanwise, w, velocity components of the modes (sampled from the case at $Re = 50$), where positive isosurfaces are colored in purple and negative isosurfaces in orange. The identification of two dominant modes common to all the low Reynolds number cases (consistent with previous stability analysis results) corroborates the unified view of EIT and ET.

by the analysis above. The frequencies of these modes are shown in Fig. 3(a) as a function of the Reynolds number, and their typical shapes are reported in Figs. 3(b) and 3(c). We observe that the fast modes are mainly located in the center of the channel, while the slow modes are localized close to the walls; their temporal frequencies do not undergo a significant variation with the Reynolds number. The modes we identify are thus unrelated to the turbulent structures observed by Choueiri *et al.* [46] in EIT, which exhibit a marked dependence on the Reynolds number and persist up to $Re = 10\,000$, yet their shapes and locations are reminiscent of the results from stability analysis [27,42] and recent simulations [19].

In this work we have simulated the turbulent flow of a viscoelastic fluid in a planar channel setup across a wide range of Reynolds numbers from TDR to ET, reporting instabilities and flow structures consistent with the available literature [9,11,27]. Our results identify two distinct turbulent regimes. First, one at large Reynolds number dominated by the turbulent shear stresses with the classical energy spectra decay predicted by Kolmogorov's theory [47] $E \sim k_x^{-5/3}$, which corresponds to the extensively investigated TDR regime [48]. Next, one at lower Reynolds number with highly elongated polymer chains producing strong polymer stresses with the energy spectra showing a fast fall-off $E \sim k_x^{-4}$, consistently with recent results in ET even at Reynolds numbers lower than those here [19,44]. We do not find any other fully developed state in between these two, and conclude that the peculiar chaotic state attained in viscoelastic planar channel flows remains unchanged by a variation in the Reynolds number once inertial effects are subdominant. Thus, within this setup, fully developed EIT [9] below $Re \approx 2800$ and ET [49] share a similar structure.

The research was supported by the Okinawa Institute of Science and Technology Graduate University (OIST) with subsidy funding to M.E.R. from the Cabinet Office, Government of Japan. Part of this work was done during the 2023 Madrid Turbulence Workshop, organized by Prof. J. Jiménez and made possible by ERC, Caust Grant ERC-AdG-101018287. M.E.R. acknowledges funding from the Japan Society for the Promotion of Science (JSPS), Grants No. 24K17210 and No. 24K00810. All authors acknowledge the computational resources provided by the Scientific

Computing section of the Research Support Division at OIST and by RIKEN, under the HPCI System Research Project Grants No. hp220099 and No. hp210269. M.E.R. and G.F.R. acknowledge the insightful discussion with Prof. R.R. Kerswell and Dr. M. Beneitez at the University of Cambridge.

Data availability. Data required to reproduce the figures are available in the website of the Complex Fluids and Flows Unit at OIST [50].

[1] A. D. Stroock, S. K. W. Dertinger, A. Ajdari, I. Mezić, H. A. Stone, and G. M. Whitesides, Chaotic mixer for microchannels, Science **295**, 647 (2002).
[2] T. J. Ober, D. Foresti, and J. A. Lewis, Active mixing of complex fluids at the microscale, Proc. Natl. Acad. Sci. USA **112**, 12293 (2015).
[3] J. Y. Han, J. N. La Fiandra, and D. L. DeVoe, Microfluidic vortex focusing for high throughput synthesis of size-tunable liposomes, Nat. Commun. **13**, 6997 (2022).
[4] A. M. Vargason, A. C. Anselmo, and S. Mitragotri, The evolution of commercial drug delivery technologies, Nat. Biomed. Eng. **5**, 951 (2021).
[5] P. Yager, T. Edwards, E. Fu, K. Helton, K. Nelson, M. R. Tam, and B. H. Weigl, Microfluidic diagnostic technologies for global public health, Nature (London) **442**, 412 (2006).
[6] A. Groisman and V. Steinberg, Efficient mixing at low Reynolds numbers using polymer additives, Nature (London) **410**, 905 (2001).
[7] F. Serafini, F. Battista, P. Gualtieri, and C. M. Casciola, Drag reduction in turbulent wall-bounded flows of realistic polymer solutions, Phys. Rev. Lett. **129**, 104502 (2022).
[8] A. Groisman and V. Steinberg, Stretching of polymers in a random three-dimensional flow, Phys. Rev. Lett. **86**, 934 (2001).
[9] Y. Dubief, V. E. Terrapon, and B. Hof, Elasto-inertial turbulence, Annu. Rev. Fluid Mech. **55**, 675 (2023).
[10] D. Samanta, Y. Dubief, M. Holzner, C. Schäfer, A. N. Morozov, C. Wagner, and B. Hof, Elasto-inertial turbulence, Proc. Natl. Acad. Sci. USA **110**, 10557 (2013).
[11] J. Page, Y. Dubief, and R. R. Kerswell, Exact traveling wave solutions in viscoelastic channel flow, Phys. Rev. Lett. **125**, 154501 (2020).
[12] M. Khalid, V. Shankar, and G. Subramanian, Continuous pathway between the elasto-inertial and elastic turbulent states in viscoelastic channel flow, Phys. Rev. Lett. **127**, 134502 (2021).
[13] P. Garg, I. Chaudhary, M. Khalid, V. Shankar, and G. Subramanian, Viscoelastic pipe flow is linearly unstable, Phys. Rev. Lett. **121**, 024502 (2018).
[14] S. Berti and G. Boffetta, Elastic waves and transition to elastic turbulence in a two-dimensional viscoelastic Kolmogorov flow, Phys. Rev. E **82**, 036314 (2010).
[15] R. B. Bird, *Dynamics of Polymeric Liquids, Volume 1: Fluid Mechanics* (Wiley, 1987).
[16] N. K. Jha and V. Steinberg, Elastically driven Kelvin–Helmholtz-like instability in straight channel flow, Proc. Natl. Acad. Sci. USA **118**, e2105211118 (2021).
[17] Y. Li and V. Steinberg, Mechanism of vorticity amplification by elastic waves in a viscoelastic channel flow, Proc. Natl. Acad. Sci. USA **120**, e2305595120 (2023).
[18] J. Song, N. Liu, X. Lu, and B. Khomami, Direct numerical simulation of elastic turbulence in the Taylor–Couette flow: Transition pathway and mechanistic insight, J. Fluid Mech. **949**, A49 (2022).
[19] M. Lellep, M. Linkmann, and A. Morozov, Purely elastic turbulence in pressure-driven channel flows, Proc. Natl. Acad. Sci. USA **121**, e2318851121 (2024).
[20] G. Boffetta, A. Celani, A. Mazzino, A. Puliafito, and M. Vergassola, The viscoelastic Kolmogorov flow: Eddy viscosity and linear stability, J. Fluid Mech. **523**, 161 (2005).
[21] A. Bistagnino, G. Boffetta, A. Celani, A. Mazzino, A. Puliafito, and M. Vergassola, Nonlinear dynamics of the viscoelastic Kolmogorov flow, J. Fluid Mech. **590**, 61 (2007).
[22] S. Berti, A. Bistagnino, G. Boffetta, A. Celani, and S. Musacchio, Two-dimensional elastic turbulence, Phys. Rev. E **77**, 055306(R) (2008).

[23] S. Sid, V. E. Terrapon, and Y. Dubief, Two-dimensional dynamics of elasto-inertial turbulence and its role in polymer drag reduction, Phys. Rev. Fluids **3**, 011301(R) (2018).
[24] Y. Dubief, J. Page, R. R. Kerswell, V. E. Terrapon, and V. Steinberg, First coherent structure in elasto-inertial turbulence, Phys. Rev. Fluids **7**, 073301 (2022).
[25] G. Buza, M. Beneitez, J. Page, and R. R. Kerswell, Finite-amplitude elastic waves in viscoelastic channel flow from large to zero Reynolds number, J. Fluid Mech. **951**, A3 (2022).
[26] A. Morozov, Coherent structures in plane channel flow of dilute polymer solutions with vanishing inertia, Phys. Rev. Lett. **129**, 017801 (2022).
[27] M. Beneitez, J. Page, and R. R. Kerswell, Polymer diffusive instability leading to elastic turbulence in plane Couette flow, Phys. Rev. Fluids **8**, L101901 (2023).
[28] A. Peterlin, Hydrodynamics of macromolecules in a velocity field with longitudinal gradient, J. Polym. Sci., Part B: Polym. Lett. **4**, 287 (1966).
[29] D. Vincenzi, S. Jin, E. Bodenschatz, and L. R. Collins, Stretching of polymers in isotropic turbulence: A statistical closure, Phys. Rev. Lett. **98**, 024503 (2007).
[30] See Supplemental Material at http://link.aps.org/supplemental/10.1103/PhysRevFluids.9.L122602 for technical details on the numerical methods. There, we also provide further insight on the flow statistics, elucidate the calibration of the modal decomposition algorithm, and investigate the dependence of the results from the polymer concentration, which includes Refs. [7,9,19,24,25,27,31–42].
[31] M. S. Abdelgawad, I. Cannon, and M. E. Rosti, Scaling and intermittency in turbulent flows of elastoviscoplastic fluids, Nat. Phys. **19**, 1059 (2023).
[32] J. Kim and P. Moin, Application of a fractional-step method to incompressible Navier-Stokes equations, J. Comput. Phys. **59**, 308 (1985).
[33] R. Fattal and R. Kupferman, Time-dependent simulation of viscoelastic flows at high Weissenberg number using the log-conformation representation, J. Non-Newtonian Fluid Mech. **126**, 23 (2005).
[34] F. De Vita, M. E. Rosti, D. Izbassarov, L. Duffo, O. Tammisola, S. Hormozi, and L. Brandt, Elastoviscoplastic flows in porous media, J. Non-Newtonian Fluid Mech. **258**, 10 (2018).
[35] K. Sugiyama, S. Ii, S. Takeuchi, S. Takagi, and Y. Matsumoto, A full Eulerian finite difference approach for solving fluid–structure coupling problems, J. Comput. Phys. **230**, 596 (2011).
[36] M. Beneitez, J. Page, Y. Dubief, and R. R. Kerswell, Multistability of elasto-inertial two-dimensional channel flow, J. Fluid Mech. **981**, A30 (2024).
[37] E. De Angelis, C. M. Casciola, and R. Piva, DNS of wall turbulence: Dilute polymers and self-sustaining mechanisms, Comput. Fluids **31**, 495 (2002).
[38] S. B. Pope, *Turbulent Flows* (Cambridge University Press, Cambridge, UK, 2000).
[39] J. M. Vega and S. Le Clainche, *Higher Order Dynamic Mode Decomposition and Its Applications* (Elsevier Science, Cambridge, MA, 2020).
[40] P. J. Schmid, Dynamic mode decomposition of numerical and experimental data, J. Fluid Mech. **656**, 5 (2010).
[41] M. M. P. Couchman, M. Beneitez, J. Page, and R. R. Kerswell, Inertial enhancement of the polymer diffusive instability, J. Fluid Mech. **981**, A2 (2024).
[42] G. Buza, J. Page, and R. R. Kerswell, Weakly nonlinear analysis of the viscoelastic instability in channel flow for finite and vanishing Reynolds numbers, J. Fluid Mech. **940**, A11 (2022).
[43] S. Tardu, *Transport and Coherent Structures in Wall Turbulence* (John Wiley & Sons, Hoboken, NJ, London, UK, 2014).
[44] R. K. Singh, P. Perlekar, D. Mitra, and M. E. Rosti, Intermittency in the not-so-smooth elastic turbulence, Nat. Commun. **15**, 4070 (2024).
[45] M. Khalid, I. Chaudhary, P. Garg, V. Shankar, and G. Subramanian, The centre-mode instability of viscoelastic plane Poiseuille flow, J. Fluid Mech. **915**, A43 (2021).
[46] G. H. Choueiri, J. M. Lopez, A. Varshney, S. Sankar, and B. Hof, Experimental observation of the origin and structure of elastoinertial turbulence, Proc. Natl. Acad. Sci. USA **118**, e2102350118 (2021).

[47] A. N. Kolmogorov, The local structure of turbulence in an incompressible viscous fluid for very large Reynolds numbers, Dokl. Akad. Nauk. SSSR **30**, 301 (1941).
[48] J. L. Lumley, Drag reduction by additives, Annu. Rev. Fluid Mech. **1**, 367 (1969).
[49] V. Steinberg, Elastic turbulence: An experimental view on inertialess random flow, Annu. Rev. Fluid Mech. **53**, 27 (2021).
[50] https://www.oist.jp/research/research-units/cffu/publications/publication-data.